Tomographic image reconstruction from continuous projections

Jeroen Cant, Willem Jan Palenstijn, Gert Behiels, Jan Sijbers

***Abstract*—An important design aspect in tomographic image reconstruction is the choice between a step-and-shoot protocol versus continuous X-ray tube movement for image acquisition. A step-and-shoot protocol implies a perfectly still tube during X-ray exposure, and hence involves moving the tube to its next position only in between exposures.**

In a continuous movement protocol, the tube is in a constant motion. The angular integration of the rays inherently produces blurred projections. Conventional reconstruction from such projections leads to blurred reconstructed images, and therefore the projection angles are kept small. Important advantages of a continuous scanning protocol are shorter acquisition times and less demands on modality construction from a mechanical point of view.

In this work, the continuous protocol is extended with continuous projections, in which the X-ray source is continuously emitting X-rays over larger angles. The focal spot motion can no longer be ignored and is modeled in the reconstruction. The reconstruction quality is compared with the equivalent step-and-shoot counterpart showing improved results for region of interest tomography.

I. Introduction

X-ray projections for tomographic image reconstruction can be acquired in different ways. In a *step-and-shoot* protocol, the X-ray tube and detector are stationary during the X-ray projection and move to a next location only in between exposures [1]. While this protocol is the easiest from an image reconstruction point of view, it poses severe constraints on the design of the modality and typically leads to a longer acquisition time.

In the *continuous* acquisition mode, the tube is in a constant motion and projections are acquired over small angles. In a spiral CT scanner, the X-ray tube and the table are in a constant motion. This enables a heavily reduced acquisition time compared to the original step-and-shoot modality [2]. For breast tomosynthesis, the tube is in a continuous movement and emits short X-ray bursts at specific intervals, which also enables a shorter acquisition time and thus increases patient comfort [3].

Most reconstruction algorithms applied to projection data that are acquired in a continuous acquisition mode, however, still assume a stationary source and detector during exposure. Any focal spot movement during exposure is considered unwanted because the angular integration of X-rays produces blurring in the projections which leads to decreased image quality. Protocols are designed in such a way that this effect is limited as much as possible, either by a low tube rotation speed or short exposure time [3] [4].

In this work, the continuous acquisition model is taken one step further. *Continuous exposures* are studied, whereby the X-ray tube *continuously* emits radiation over larger angles while moving through the acquisition path. In this model, focal spot motion can no longer be neglected and needs to be modeled in the reconstruction.

Motion related reconstruction artifacts have already been studied extensively in the literature. Object motion during acquisition of the different projections creates inconsistencies between the projection images, leading to reconstruction artifacts unless the motion is modeled and incorporated in the reconstruction algorithm [5]. A common example of subject motion occurs in imaging of a thorax when a patient cannot hold his breath. Another motion related artifact is caused by unwanted motion of the tube or detector, e.g., due to mechanical drifting [6]. The focal spot motion of the continuous exposures, however, differs from the previous motion examples as it is incorporated into the acquisition protocol by design. Recently, investigations have been made for modeling small focal spot motion to improve reconstruction quality in breast tomosynthesis [7].

In our work, the effect on the image quality of reconstructions modeling continuous exposures is studied and compared with reconstructions from a step-and-shoot model with equal total radiation dose and number of projections. As will be demonstrated, for specific applications such as region of interest tomography, reconstructions from continuous exposures may significantly improve the image quality of the equivalent step-and-shoot protocol, at the cost of decreasing spatial resolution outside the region of interest.

The concept of continuous projections and the integration in the SIRT algorithm is worked out in section II. In section III the Fourier sampling behaviour of the continuous projections is analysed. Section IV contains experiments on various phantoms. The conclusion can be found in section V.

II. Methods

In this section, the concept of continuous projections is explained for parallel beam geometry. Generalization to other geometries is straightforward.

A. Continuous projections

The attenuation of an X-ray beam in the case of a step-and-shoot protocol, further referred to as a '*static*' projection, can

JC, WJP and JS are with the iMinds-Vision Lab, University of Antwerp, Belgium. JC and GB are with Agfa Healthcare NV, Belgium. Corresponding author: jeroen.cant2@uantwerpen.be

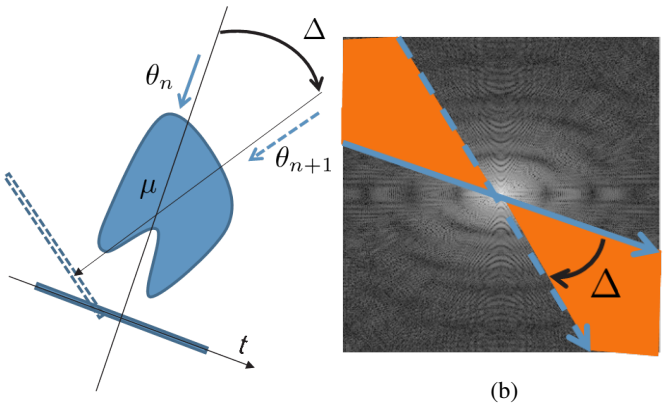

(a) (b)

Fig. 1: (a) shows an example image acquisition geometry. Parallel beam projections are acquired at angles $\theta_n = n\Delta$ with $n = 1, ..., N$. (b) shows the corresponding lines of these projections in the Fourier space. In a *continuous* acquisition, the detector integrates photons between θ_n and θ_{n+1} and hence gathers information about a wedge of angular width Δ in the Fourier space.

be expressed as follows:

$$I_n^s(t) = I_0 \exp\left(-\int_{L_{t,\theta_n}} \mu(x,y)ds\right) \tag{1}$$

with $(x, y) = (r\cos\theta_n - s\sin\theta_n, r\sin\theta_n + s\cos\theta_n)$. Furthermore, I_0 is the intensity measured by the detector without object and I the intensity after attenuation by the object. The attenuation coefficients of the imaged object are represented by $\mu(x, y)$, and the line integral is taken over the X-ray beam L_{t,θ_n} from source to detector as illustrated in Fig. 1a.

After dividing the projection data by I_0, taking the logarithm and inversion, the discretized version of Eq. (1) can be expressed as a linear combination of the attenuation coefficients in $\mathbf{x}$ along the path of the ray:

$$b_i = \sum_j a_{i,j}x_j \tag{2}$$

where b_i represents projection pixel i. The image vector $\mathbf{x}$ is the discrete representation of μ, and the weight of the attenuation coefficient at image pixel x_j is $a_{i,j}$, which is related to the intersection length of the ray with this pixel.

The combination of Eq. (2) for all projection pixels leads to a system of linear equations

$$\mathbf{b} = \mathbf{A}\mathbf{x} \tag{3}$$

where $\mathbf{A} = \{a_{i,j}\}$ represents the system matrix, $\mathbf{x}$ the vector of unknown attenuation coefficients in the discrete representation of μ and $\mathbf{b}$ the vector of the entire projection data.

In case of *continuous* projections, each projection value $I_n^c(t)$ is the result of the integration of photons during rotation of the source-detector system from θ_n to $\theta_{n+1} = \theta_n + \Delta$. When the same total radiation dose is administered and the X-ray source and detector move with constant angular velocity, the measured intensity is given by:

$$I_n^c(t) = \frac{I_0}{\Delta}\int_{\alpha=\theta_n}^{\theta_{n+1}} \exp\left(-\int_{L_{t,\alpha}} \mu(x,y)ds\right)d\alpha. \tag{4}$$

with $(x, y) = (r\cos\alpha - s\sin\alpha, r\sin\alpha + s\cos\alpha)$. For simplicity, the tube is assumed to emit a constant intensity. Also, the delay for reading out the detector is neglected. A more refined model for the emitted energy is presented by [7].

To obtain a discrete formulation of Eq. (4), S rays are sampled between θ_n and θ_{n+1}. Eq. (2) is modified to:

$$b_i = -\log\left(\frac{1}{S}\sum_{s=0}^{S-1}\exp\left[-\sum_j a_{i,j,s}x_j\right]\right) \tag{5}$$

where $a_{i,j,s}$ now represents the weight of the attenuation coefficient at position j for the beam arriving at detector pixel i with angle $\theta_n + \frac{s}{S}\Delta$.

The sampling factor S should be chosen high enough to correctly sample the full area between the corresponding lines in the Fourier space as illustrated in Fig. 1b. The coefficients $a_{i,j,s}$ can be obtained by modelling the sampled continuous projections system as a static projections system with $S \times N$ projections.

B. Continuous SIRT

The system of equations (3) can be solved using the well known Simultaneous Iterative Reconstruction Technique (SIRT) algorithm, which can be written in matrix formulation as [8]:

$$\mathbf{x}^{(k+1)} = \mathbf{x}^{(k)} + \mathbf{C}\mathbf{A}^T\mathbf{R}(\mathbf{b} - \mathbf{A}\mathbf{x}^{(k)}),$$

where $\mathbf{x}^k$ represents the reconstructed image at iteration k and $\mathbf{C}$ and $\mathbf{R}$ the diagonal matrices with the inverse column and row sums of the system matrix $\mathbf{A}$, respectively. The operation $\mathbf{A}\mathbf{x}^{(k)}$ corresponds to a so called *forward projection*, and the transpose $\mathbf{A}^T$ is referred to as the *backprojection* operator. With static exposures, this forward projection comes down to a weighted sum of image pixel values on a ray from source to detector, using an interpolation scheme between all pixels that are partially intersected by this ray. Similarly, the backprojection is a weighted redistribution of a value across the same image pixels in the neighbourhood of that ray.

For the protocol with continuous projections, the forward and backward projectors are adapted. Instead of backprojecting a value along a single ray, this value is distributed across S rays corresponding to S source-detector positions of each exposure. The forward projector is modeled by S rays matching our sampled continuous exposure.

III. Fourier analysis

For a parallel beam geometry, the effect of uniformly moving the source while constantly emitting radiation can intuitively be understood from the fourier-slice theorem . This theorem states that for parallel beams, the Fourier transform of a static projection $p(x)$ of an image $f(x)$ is equal to a slice $s(k_x)$ in F, the Fourier transform of f. Stated otherwise,

each projection p 'samples' the Fourier space F of our image formed by the attenuation coefficients μ.

Where static projections represent lines in the Fourier space, a *continuous* projection will integrate all rays between angles θ_n and θ_{n+1} and thus gather information from the entire area in the Fourier space between the two corresponding lines of the static projections (Fig. 1b).

Conceptually, one can easily understand that when acquiring only a few static projection images, the Fourier space of the image will be severely undersampled and hence the reconstructed image will contain reconstruction artifacts. This can be seen in Fig. 2, where the reconstruction from only 10 projections shows streak artifacts.

Since the continuous projections sample the whole area between the corresponding lines of the start and end angle in the Fourier space of the image, it can be expected that this technique produces reconstructions with less streak artifacts. In the following section the reconstruction algorithm based on these continuous projections is compared with static reconstruction algorithms under various circumstances.

(a) Phantom (b) 180 projections (c) 10 projections

Fig. 2: SIRT reconstructions of a Shepp-Logan phantom (a) with 180 (b) and 10 (c) projections, showing typical streak artifacts.

IV. Experiments

A. Reconstruction comparison between static and continuous projections.

To illustrate the effect of continuous vs static projections, the root mean square error (RMSE) for SIRT reconstructions from static and continuous projections on the Shepp-Logan phantom was compared as a function of the number of projections. The static projections were equally distributed along 180 degrees and the continuous projections integrated all rays between two consecutive static projections. 1000 iterations were performed for all reconstructions. The SIRT algorithm used for the continuous projections was modified as described in section II-B by sampling the rays in the angular range of the projections. For a limited number of projections, the continuous exposures resulted in a lower RMSE. With increasing number of projections, the difference between both methods vanished (see Fig. 3).

The continuous projections approach was also applied to the XCAT [9] phantom, with the center of source-detector rotation in the left lung. One can easily notice from Fig. 5 that the resolution improved in the rotation center, but decreased with increasing distance from this rotation center compared to the static reconstruction. This suggests that continuous projections might be of use in region of interest tomography, e.g., during surgery when a physician is only interested in a fast and accurate reconstruction of a local region of the patient.

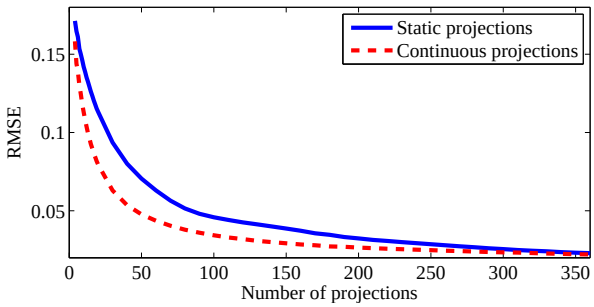

Fig. 3: RMSE for SIRT reconstructions in function of the number of projections. All projections angles were distributed evenly over a total acquisition angle of 180 degrees.

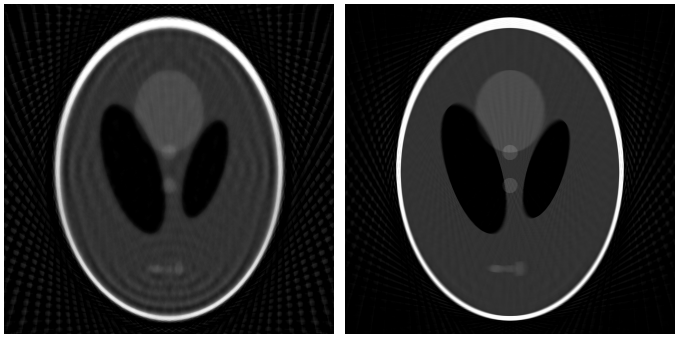

(a) static (b) continuous

Fig. 4: Reconstruction of the Shepp Logan phantom, using 45 static (a) and continuous (b) projections.

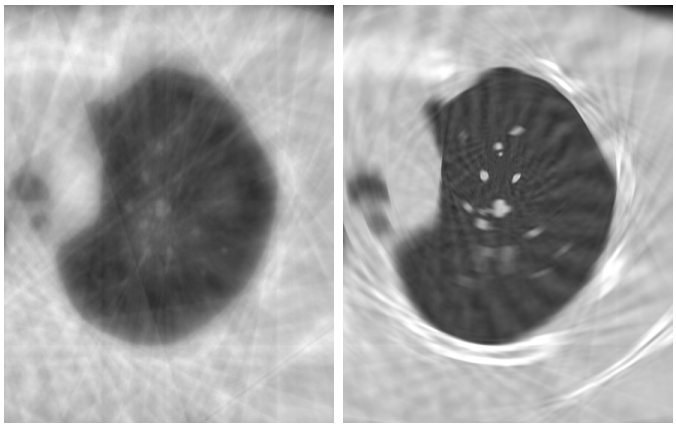

(a) static (b) continuous

Fig. 5: Reconstruction of the XCAT phantom, using only 20 static (a) and fully continuous (b) projections with rotation center in left lung. Both images are displayed with equal contrast settings.

Besides an improved image quality around the rotation center, artifacts can be observed due to the motion of the tube outside this center. To analyze this further, projections of

two phantoms were reconstructed. The first phantom (Fig. 6a) consists of concentric circles, centered in the tube-detector rotation center. In Fig. 6b & 6c, reconstructions from 20 static projections and 20 continuously acquired exposures are shown, respectively. Whereas the static reconstruction shows many artifacts, the continuous reconstruction is nearly perfect.

The second phantom in Fig. 6d consists of 10 radial lines, distributed evenly over 360°. The reconstruction from 20 continuous projections in Fig. 6f smeared the radial lines along concentric circles, centered in the tube-detector rotation center. The angle of this smearing corresponds to the covered angle of the continuous projections.

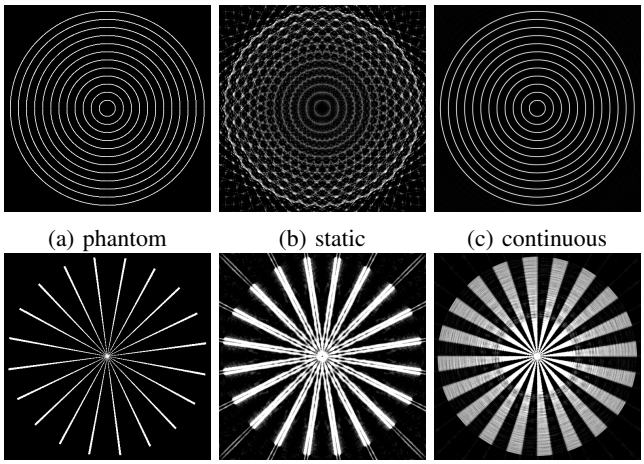

(a) phantom (b) static (c) continuous

(d) phantom (e) static (f) continuous

Fig. 6: Circles phantom (a) with static (b) and continuous (c) reconstruction, showing nearly perfect reconstruction for the continuous projections. The radial lines phantom (d) illustrates the concentric nature of the artifacts in continuous reconstruction (f). Contrast was enhanced in all images for easier visibility.

B. Noisy projections

The previous experiments were performed with noiseless projections. As noiseless imaging is not a realistic scenario, the effect of adding Poisson noise in the sinograms on the reconstruction quality of continuous projections was investigated. Reconstructions of static and fully continuous projections were compared, both methods using the same radiation dose per projection and an equal number of projections.

The artifacts along arcs centered around the tube-detector rotation center, as discussed in section IV-A, can also be seen in the continuous reconstruction from noisy projections (see Fig. 7).

V. Conclusion

An acquisition protocol was investigated with continuous exposures involving an X-ray source that continuously moves while continuously emitting radiation. The motion of the X-ray source was modeled in the reconstruction algorithm. A comparison with a conventional step-and-shoot acquisition protocol using the same total radiation dose and number of projections showed reduced artifacts and improved contrast and resolution around the tube-detector rotation center.

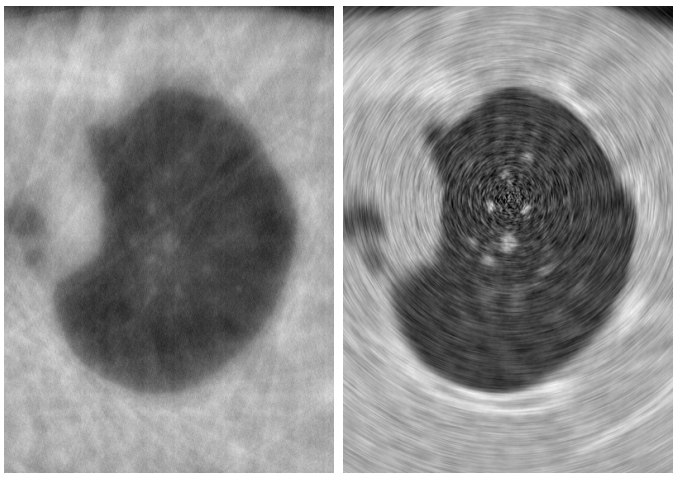

(a) static (b) continuous

Fig. 7: Reconstruction of the XCAT phantom, using 20 static (a) and fully continuous (b) noisy projections. We have used 300 iterations of SIRT used in both cases. Both images are displayed with equal contrast settings.

Acknowledgement

This work was funded by the Agency for Innovation by Science and Technology in Flanders (IWT). Networking support was provided by the EXTREMA COST Action MP1207.

References

[1] J. Hsieh, J. Londt, M. Vass, J. Li, X. Tang, and D. Okerlund, "Step-and-shoot data acquisition and reconstruction for cardiac x-ray computed tomography," *Medical Physics*, vol. 33, no. 11, p. 4236, 2006.

[2] W. A. Kalender, W. Seissler, and P. Vock, "Single-breath-hold spiral volumetric ct by continuous patient translation and scanner rotation," *Radiology*, vol. 173, no. 2, p. 414, 1989.

[3] A. Smith, "Fundamentals of breast tomosynthesis," *White Paper, Hologic Inc., WP-00007*, 2008.

[4] H. U. Kerl, C. T. Isaza, H. Boll, S. J. Schambach, I. S. Nolte, C. Groden, and M. a. Brockmann, "Evaluation of a continuous-rotation, high-speed scanning protocol for micro-computed tomography." *Journal of computer assisted tomography*, vol. 35, no. 4, pp. 517–23, 2011.

[5] I. Al-Shakhrah and T. Al-Obaidi, "Common artifacts in computerized tomography: A review," *Applied Radiology*, vol. 32, no. 8, pp. 25–32, 2003.

[6] W. A. Kalender and Y. Kyriakou, "Flat-detector computed tomography (FD-CT)." *European radiology*, vol. 17, no. 11, pp. 2767–79, Nov. 2007.

[7] K. Michielsen, K. Van Slambrouck, A. Jerebko, and J. Nuyts, "Patchwork reconstruction with resolution modeling for digital breast tomosynthesis," *Medical Physics*, vol. 40, no. 3, pp. 1–10, 2013.

[8] J. Gregor and T. Benson, "Computational analysis and improvement of SIRT." *IEEE transactions on medical imaging*, vol. 27, no. 7, pp. 918–24, Jan. 2008.

[9] W. P. Segars, M. Mahesh, T. J. Beck, E. C. Frey, and B. M. W. Tsui, "Realistic ct simulation using the 4d xcat phantom," *Medical physics*, vol. 35, no. 8, pp. 3800–3808, 2008.